Sensors and Materials, Vol. 37, No. 2 (2025) 497–508
MYU Tokyo

S & M 3925

Radiation-induced Luminescence Characteristics of Ce-doped La_2O_3–Al_2O_3 Glasses Prepared by Gas Levitation Furnace

Daiki Shiratori,[1*] Atsunobu Masuno,[2] Takumi Kato,[3]
Yutaka Fukuchi,[1] and Takayuki Yanagida[3]

[1]Faculty of Engineering, Tokyo University of Science, 6-3-1 Niijuku, Katsushika-ku, Tokyo 125-8585, Japan
[2]Graduate School of Engineering, Kyoto University, Kyotodaigaku-Katsura, Nishikyo-ku, Kyoto 615-8520, Japan
[3]Guraduate School of Science and Technology, Nara Institute of Science and Technology,
8916-5 Takayama, Ikoma, Nara 630-0192, Japan

(Received October 31, 2024; accepted December 24, 2024)

Keywords: glass, phosphor, scintillation, dosimeter, photoluminescence

In this study, Ce-doped La_2O_3–Al_2O_3 glasses were prepared by the levitation method, a containerless glass-making method, and their optical and radiation-induced luminescence properties were investigated. From the Raman spectral analysis, it was observed that an increase in La_2O_3 content correlates with an increase in the number of non-bridging oxygen (NBO) atoms arising from the reduction in the number of AlO_4 units, and a decrease in the number of high-coordination aluminum species such as AlO_5 and AlO_6. Variations in glass composition also affect the luminescent properties. In samples with lower La_2O_3 content, two types of emission were observed: one from typical Ce^{3+} ions and the other from Ce–O associates. However, as the La_2O_3 content increased, the emission from Ce–O associates diminished and ultimately disappeared. In the scintillation spectra, the luminescence from Ce–O associates was barely observed, whereas that from the 5*d*–4*f* transition of Ce^{3+} was dominant. Since the emission intensity is affected by the number of carrier traps, the Ce-doped La_2O_3–Al_2O_3 glass can function as both a scintillator and a dosimeter material by optimizing the glass composition.

1. Introduction

Radiation detectors have an extensive range of applications in modern society: nuclear medicine,[1–3] high-energy astronomy,[4–6] environmental dose monitoring,[7,8] personal dose monitoring,[9,10] security,[11–13] and well logging.[14–16] In most of these applications, radiation detectors using phosphors (scintillators and dosimeter materials) are employed. Scintillators are materials that exhibit prompt luminescence upon radiation exposure,[17–21] making them suitable for real-time measurements in devices such as positron emission tomography and computed tomography scanners in medical settings and baggage inspection systems at airports. On the other hand, dosimeter materials accumulate radiation energy once as carriers and read it out later as photoluminescence (PL). There are two types of dosimeter classified by different ways (energies) to stimulate carriers: the thermally stimulated luminescence (TSL) dosimeter using

*Corresponding author: e-mail: shiratori@rs.tus.ac.jp
https://doi.org/10.18494/SAM5439

ISSN 0914-4935
https://myukk.org/

thermal stimulation[22–27] and the optically stimulated luminescence (OSL) dosimeter utilizing light stimulation.[28–32] Various materials have been developed for radiation detection, with aluminates recognized as relatively effective radiation-induced luminescent materials. Notable examples of scintillators include Ce:$Y_3Al_5O_{12}$,[33] Ce:$Lu_3Al_5O_{12}$,[34] and Ce:$LuAlO_3$.[35] As dosimeter materials, Ce,Dy:$LaAlO_3$ and C:$LaAlO_3$ are representative examples.[36–38] On the other hand, these are all reports on crystalline or ceramic materials, and there have been no studies in glass form. Glass phosphors offer advantages such as high transparency, ease of processing, and high luminescence efficiency, making them highly industrially valuable. Recently, they have attracted significant attention for use as color converters in white light emitting diodes (WLEDs).[39–41] Naturally, interest in glass phosphors extends to radiation detection as well, where extensive research is focused on developing high-performance glass scintillators and glass dosimeters. The extensive applications of glass materials across various fields are indeed due to recent rapid advancements in glass synthesis and analysis techniques. Notably, the containerless glass-making method, known as the crucible-free technique, has opened possibilities for new materials by enabling the vitrification of compositions without glass-forming oxides, which were previously deemed unachievable.[42,43] This approach has significantly expanded the potential applications for glass materials. Our research interest lies in examining the properties of aluminate-based materials, traditionally challenging to vitrify and previously explored only in crystalline form for radiation-induced luminescence. As a first step, we focused on the La_2O_3–Al_2O_3 binary system and investigated its scintillation and dosimeter properties.

2. Materials and Methods

2.1 Preparation method

Ce:La_2O_3–Al_2O_3 glasses were prepared by a levitation technique using an aerodynamic levitation (ADL) furnace.[43] The starting materials of La_2O_3 (4N, Rare Metallic), Al_2O_3 (4N, Taimei Chemicals), and CeO_2 (4N, Furuuchi Chemical) powders were mixed at the molar ratio as shown in Table 1. The raw powder materials were uniformly mixed using an agate mortar, then pressed into 1-cm-diameter pellets by applying a pressure of 20 kN for 10 min using a press machine (Mini-Lab-Press, Labnect Co., Ltd.). The obtained pellets were sintered at 1200 ºC for 8 h in the air using an electric furnace to be made into ceramic pellets. After sufficient cooling, the obtained pellets were ground to pieces as targets for an ADL furnace. Targets were placed on the nozzle of the ADL furnace and levitated by O_2 gas flow, and a CO_2 laser was applied to melt

Table 1
Composition ratios of the synthesized e-doped La_2O_3–Al_2O_3 glass samples.

Sample code	La_2O_3 (mol.%)	Al_2O_3 (mol.%)	CeO_2 (mol.%)
35La65Al	35	65	1.0
40La60Al	40	60	1.0
45La55Al	45	55	1.0
50La50Al	50	50	1.0

the levitated targets. The melt was rapidly cooled to room temperature by turning off the laser power and then solidified. Optical and scintillation spectra were measured using glasses in their as-synthesized state, while glass samples were ground and processed into pellets for the TSL spectrum measurements. A mortar and pestle was used to grind the glass, and 1-cm-diameter pellets were obtained by pressurizing at 10 kN for 10 min using the press machine.

2.2 Analysis method

X-ray diffraction (XRD) patterns of the glass samples were obtained by powder X-ray diffractometry (MiniFlex600, Rigaku) with a Cu Kα source, while the operation voltage and current were set as 40 kV and 15 Ma, respectively. The Raman spectra measurements were carried out by Raman spectroscopy (RMP-500, JASCO), and the laser condition was a 532.1 nm line of a coherent laser as an excitation source operating at 20 ± 0.5 mW power. The diffuse transmission spectra were measured using a spectrophotometer (SolidSpec-3700, Shimadzu) across a spectral range from 200 to 800 nm with 1 nm intervals. We measured the optical properties of the glass samples to determine the luminescence characteristics. The PL excitation/emission spectra were obtained using a spectrofluorometer (FP-8600, JASCO) equipped with an Xe-lamp as an excitation source. PL decay curve measurements were performed using a PL lifetime measurement system Quantaurus-Tau (C11367, Hamamatsu Photonics). Scintillation spectra were measured using the original setup.[17] An X-ray generator (XRB80N100/CB, Spellman) equipped with a conventional X-ray tube was used as the X-ray source, and the operation current and tube voltage of the X-ray tube were 1.2 mA and 80 kV, respectively. The scintillation obtained by the irradiation of X-rays was guided through an optical fiber to a monochromator equipped with a charge coupled device (CCD)-based detector (163 monochromator, Shamrock and DU-420-BU2 CCD, Andor). TSL glow curves were measured using TL-2000 (Nanogray Inc.), and we set up the temperature range and heating rate to 50–490 °C and 1 °C/s, respectively.

3. Results and Discussion

Figure 1 shows photographs of the Ce-doped glass samples under WLED light. Owing to the nature of the synthesis method, the obtained glass samples are spherical and have a diameter of about 1–5 mm. All the glass samples are transparent with a slight yellowish tint.

(a) (b) (c) (d)

Fig. 1. (Color online) Photographs of Ce-doped La_2O_3–Al_2O_3 glasses under white LED light: (a) 35La65Al, (b) 40La60Al, (c) 45La55Al, and (d)50La50Al.

Figure 2 shows the XRD pattern results of each Ce-doped La_2O_3–Al_2O_3 glass powder. All samples have a broad peak around 2θ = 30 deg. The broad diffraction pattern is a halo peak unique to glass materials based on the structure of Al_2O_3, and this result suggests that the glass samples have a typical Al_2O_3-based glass network structure with shared AlO_4 units. Moreover, no diffraction peaks suggesting the presence of crystals or impurities were observed in the XRD patterns of any of the samples, indicating that La_2O_3–Al_2O_3 glasses were successfully synthesized.

Figure 3 shows Raman spectra of Ce-doped La_2O_3–Al_2O_3 glass samples. The intense bands are observed in three regions: (i) the highest wavenumber region (700–950 cm^{-1}), (ii) the middle region (500–700 cm^{-1}), and (iii) the lowest region (200–500 cm^{-1}). The intensity of band iii tends to increase with the La_2O_3 content relatively. In addition, the shoulders at 900 and 630 cm^{-1} are

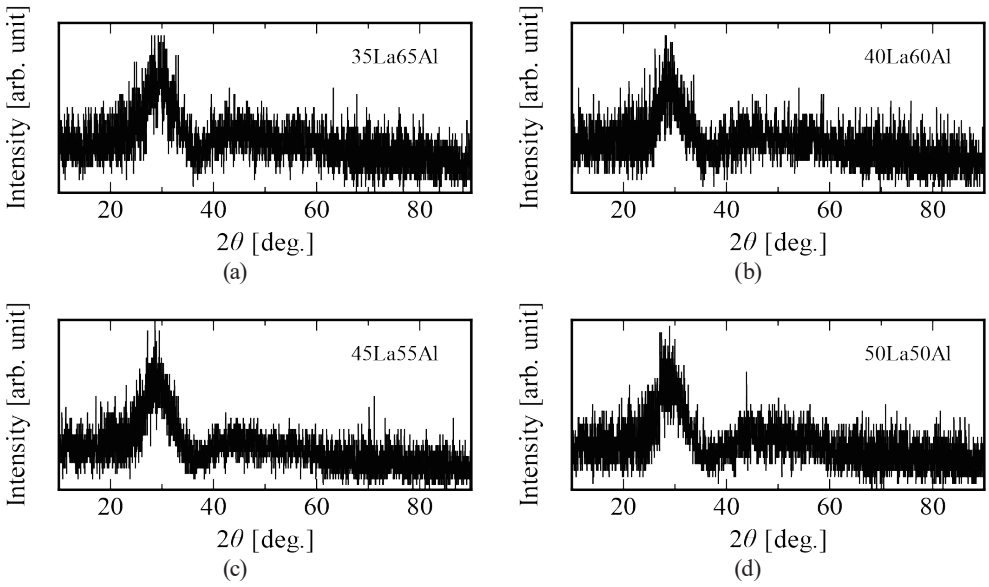

Fig. 2. XRD patterns of Ce-doped La_2O_3–Al_2O_3 glasses: (a) 35La65Al, (b) 40La60Al, (c) 45La55Al, and (d) 50La50Al.

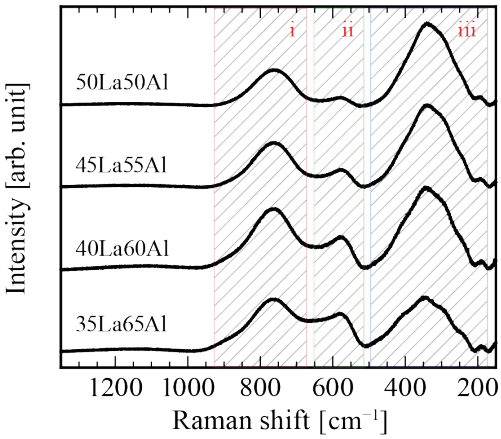

Fig. 3. (Color online) Raman spectra of Ce-doped La_2O_3–Al_2O_3 glasses.

more pronounced in samples with lower La_2O_3 content, and their intensity increases with decreasing La_2O_3 content. The main three bands at around 790, 590, and 350 are assigned to the symmetric stretching of Al–O^- with two pairs of non-bridging oxygen (NBO) atoms bonded in AlO_4,[44] the transverse motion of bridged oxygen with the Al–O–Al linkage,[45] and La-related vibrations, respectively. Band iii is a composite band made up of multiple vibrational modes. On the basis of the reported Raman spectra of La_2O_3 and La_2O_3–GeO_2–Ga_2O_3 glasses, which were obtained from thin films and polycrystalline powders, these vibrational bands are attributed to the La–O bond vibrations.[46–48] Moreover, the shoulders at around 900 and 630 cm^{-1} are attributed to the Al–O stretching vibration of the fully polymerized AlO_4 group and the vibration related to AlO_5 or higher coordinated Al.[45] Previous studies on La_2O_3–Al_2O_3 glasses have shown that with increasing La_2O_3 content, the AlO_4 network is depolymerized, which increases the number of NBO atoms.[45] The same trend was observed in these samples, suggesting that the number of NBO atoms increased with La_2O_3 content.

Figure 4 shows the diffuse transmission spectra of Ce-doped La_2O_3–Al_2O_3 glass samples. The inset highlights an enlarged view of the transmission spectrum within the 380–470 nm range. All samples exhibit high transmittance, approximately 80–90%, in the visible region between 450 and 800 nm. Variations in transmittance among the glass samples likely stem not from intrinsic glass properties, but rather from differences in sample size and measurement error. Additionally, these glasses exhibit a characteristic absorption band in the region below 400 nm. Given that the optical band gap of $28La_2O_3$–$72Al_2O_3$ glass is reported to be approximately 5.14 eV (~240 nm),[49] the observed decrease in transmittance near 400 nm is more reasonably attributed not to the optical absorption edge, but to an absorption band within the 300–400 nm range, likely associated with Ce ions. Ce ions exist in glass in either the trivalent or tetravalent state, with trivalent Ce particularly known to exhibit absorption in the UV–VIS region due to electronic transitions from the 4*f* ground state to excited 5*d* levels.[50–53] On the basis of these observations, it is reasonable to attribute the broad absorption band observed in the ultraviolet to blue regions to the 4*f*–5*d* transition of Ce^{3+} ions. In addition, no significant shift trend in absorption wavelengths with changing composition ratios was observed.

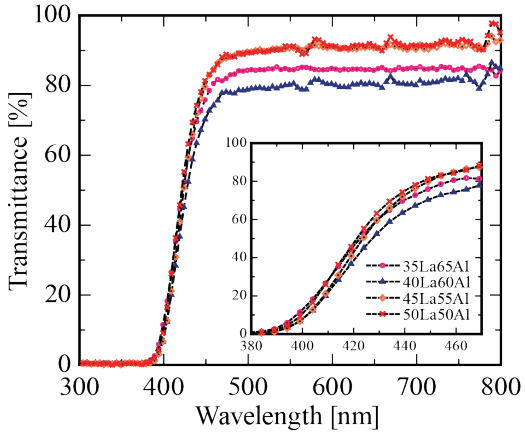

Fig. 4. (Color online) Diffuse transmission spectra of Ce-doped La_2O_3–Al_2O_3 glasses.

Figure 5 shows the PL excitation and emission spectra for each La_2O_3–Al_2O_3 glass sample. All samples exhibit broad visible emission under excitation at ~370 nm, with emission bands varying by glass composition. The 35La65Al and 40La60Al samples exhibited emission extending from 400 to 700 nm, while in the 45La55Al and 50La50Al samples, emission bands on the longer-wavelength side beyond 550 nm disappeared. To clarify the origin of these emissions, we measured PL decay curves with excitation and observation wavelengths set to 365 and 470 nm, respectively as shown in Fig. 6. The decay curves of the samples were approximated by a sum of two exponential decay functions. The approximated PL lifetimes of the glass samples from measured decay curves are summarized in Table 2. The two deduced PL lifetimes were approximately several and several tens of nanoseconds in all the samples. These findings imply that the broad emission observed in the PL spectra arises from at least two distinct

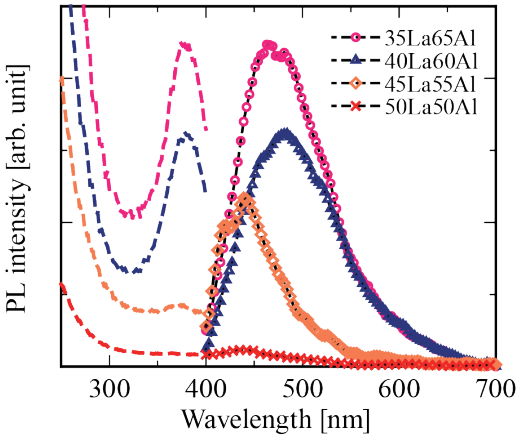

Fig. 5. (Color online) PL excitation/emission spectra of Ce-doped La_2O_3–Al_2O_3 glasses.

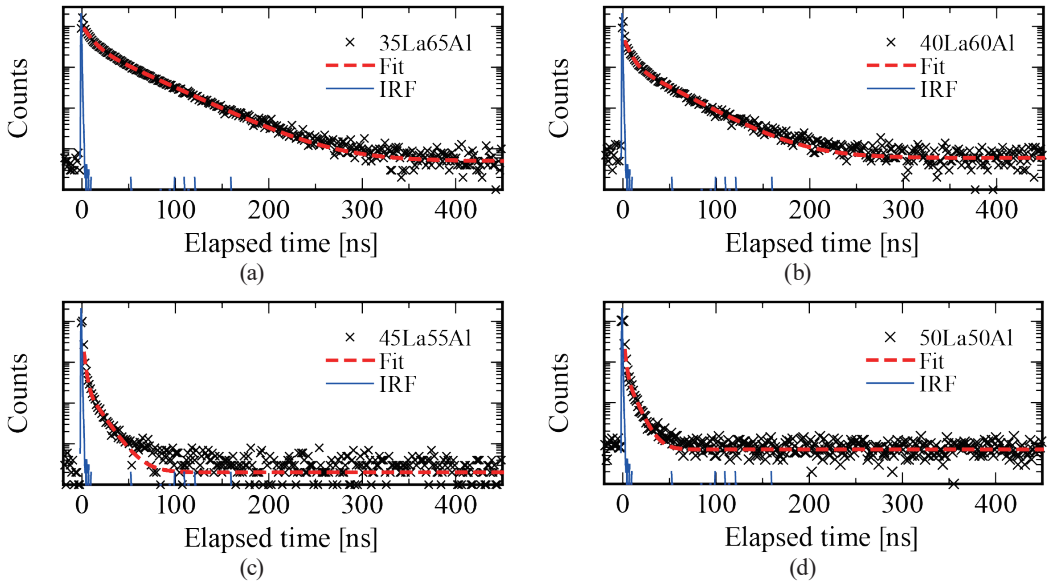

Fig. 6. (Color online) PL decay curves of Ce-doped La_2O_3–Al_2O_3 glasses. (a) 35La65Al, (b) 40La60Al, (c) 45La55Al, and (d) 50La50Al.

Table 2
PL lifetimes of Ce-doped La_2O_3–Al_2O_3 glasses. Percentages in parentheses indicate component ratios at each lifetime.

Sample code	Lifetimes τ_1 (ns)	Lifetimes τ_2 (ns)
35La65Al	9.1 (62%)	41.2 (38%)
40La60Al	6.1 (72%)	35.9 (28%)
45La55Al	2.0 (88%)	12.8 (12%)
50La50Al	1.6 (>99%)	8.3 (<1%)

luminescent centers. The lifetimes with several tens of nanoseconds (41.2–8.3 ns) are consistent with the typical values for the 5*d*–4*f* transition of Ce^{3+}, indicating that at least a portion of the observed emission originates from Ce ions. On the other hand, regarding the origin of the emission with a short lifetime of approximately 9.1–1.6 ns, it is plausible that this emission arises from Ce^{3+} ions in different coordination environments, given that both its emission wavelength and PL lifetime values are relatively close to those typical of Ce^{3+}. Here, on the basis of the results of Raman spectra in Fig. 3 and reports on the structure of La_2O_3–Al_2O_3 glasses, an increase in La_2O_3 content causes an increase in the number of NBO atoms and changes in the glass network (decrease in the number of highly coordinated Al species such as AlO_5 and AlO_6). With these structural changes, the coordination environment of Ce ions may have changed. Several reports have indicated that, in certain aluminates, including lanthanum aluminates, some of the trivalent cations are replaced by oxygen, leading to the formation of Ce–O associates.[54–56] Ce–O associates have been observed in lanthanum aluminates at Al-rich compositions such as $LaAl_{11}O_{18}$, where the emission energy is lower than that of Ce^{3+} substituting for the typical La^{3+} sites.[56] From the above findings, it is reasonable to conclude that the emission in the 400–500 nm range is attributed to typical Ce^{3+} ions with coordination environments similar to La ions, while the longer-wavelength emission (500–600 nm) is likely associated with Ce^{3+} ions in Ce–O associates. It has been shown that the oxygen coordination number of La in the $23La_2O_3$–$77Al_2O_3$ glass is approximately 6–9,[57] and there are reports indicating that the coordination number of Eu in the $50La_2O_3$–$50Al_2O_3$ glass is around 8.[58] On the basis of this, it is assumed that the coordination number of Ce ions is likely to be similar. However, the precise coordination environment of Ce ions will need to be clarified in future studies. The fact that the emission components on the longer wavelengths are more pronounced in compositions with high Al_2O_3 content also suggests the presence of Ce–O associates. The PL lifetime τ_1 assigned as the emission from Ce–O associates being considerably shorter than the typical lifetime of the Ce^{3+} ion is likely due to the lower radiative transition probability of the emission. Furthermore, the emission intensity and lifetimes t_1 and t_2 decreased with increasing La_2O_3 content, indicating that the radiative transition probability of emission due to Ce^{3+} most likely decreased with increasing La_2O_3 content.

Figure 7 shows the X-ray-induced scintillation spectra of Ce-doped La_2O_3–Al_2O_3 glasses. All samples exhibit broad emission from 400–600 nm, with an emission peak around ~450 nm. This is in contrast to the results observed in PL, where the scintillation emission is mainly due to the 5*d*–4*f* transition of Ce^{3+} ions. The variation in scintillation intensity for each sample generally aligns with the trends observed in the PL spectra, showing a decrease as La_2O_3 content increases,

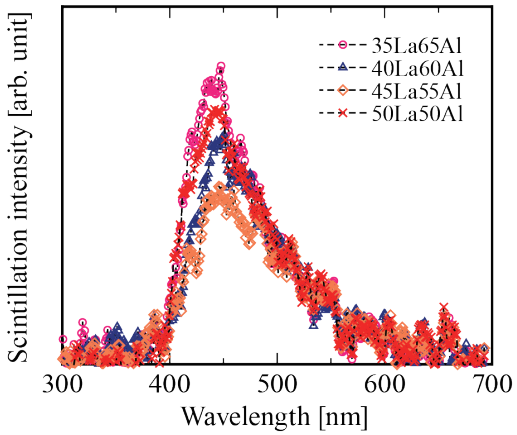

Fig. 7. (Color online) X-ray-induced scintillation spectra of Ce-doped La_2O_3–Al_2O_3 glasses.

with the exception of the 50La50Al sample. Note that the scintillation intensity of the 50La50Al sample, for which almost no emission was observed in the PL spectrum, was comparable to that of the 35La65Al sample. To further discuss these results, we measured the TSL glow curve and evaluated the number of trapping centers. Figure 8 shows the TSL glow curves of Ce-doped La_2O_3–Al_2O_3 glasses before and after X-ray irradiation. All the samples have TSL peaks at ~60 and ~350 °C, and the peak positions do not change with the composition ratio. In other words, it is suggested that the trapping centers contributing to TSL are the same in all of the glasses. Figure 9 shows the correlation of the integrated PL, scintillation, and TSL intensities as functions of La_2O_3 content of Ce-doped La_2O_3–Al_2O_3 glasses. In the 35La65Al and 40La60Al samples, scintillation and TSL intensities decrease proportionally to PL intensity, but this is not the case in the 45La55Al and 50La50Al samples. In other words, the effect of the PL quantum yield is prominent in the 35La65Al and 40La60Al samples, while the effect of the energy transport process may be dominant in the 45La55Al and 50La50Al samples. The luminescence process in radiation-induced fluorescent materials can be broadly classified into three categories: the energy conversion process, in which electrons are generated by absorbing radiation energy; the energy transport process, in which the generated electrons are transported to the emission center; and the luminescence process, in which scintillation, TSL, and OSL occur at the emission center. Whether a material exhibits scintillation or storage-type luminescence depends on the bifurcation of whether electrons are captured or not during the energy transport process, and it is known that there is an anti-correlation between them. As suggested by the Raman spectra shown in Fig. 3 and the analysis results from previous nuclear magnetic resonance (NMR) and Raman spectroscopic studies,[45] changes in glass composition lead to significant structural changes in the glass network. These structural changes may result in a substantial increase in the number of electron trapping centers owing to the formation of defects and other related factors. However, further investigation is required to elucidate the actual underlying causes. On the other hand, as the La_2O_3 ratio rises from 45 to 50, the number of trapping centers appears to decrease, thereby enhancing energy transfer efficiency within the scintillation process and consequently increasing scintillation intensity. One factor that may contribute to the reduction in the number of defects in the 50La50Al sample is that its stoichiometric ratio matches that of $LaAlO_3$. It is known that

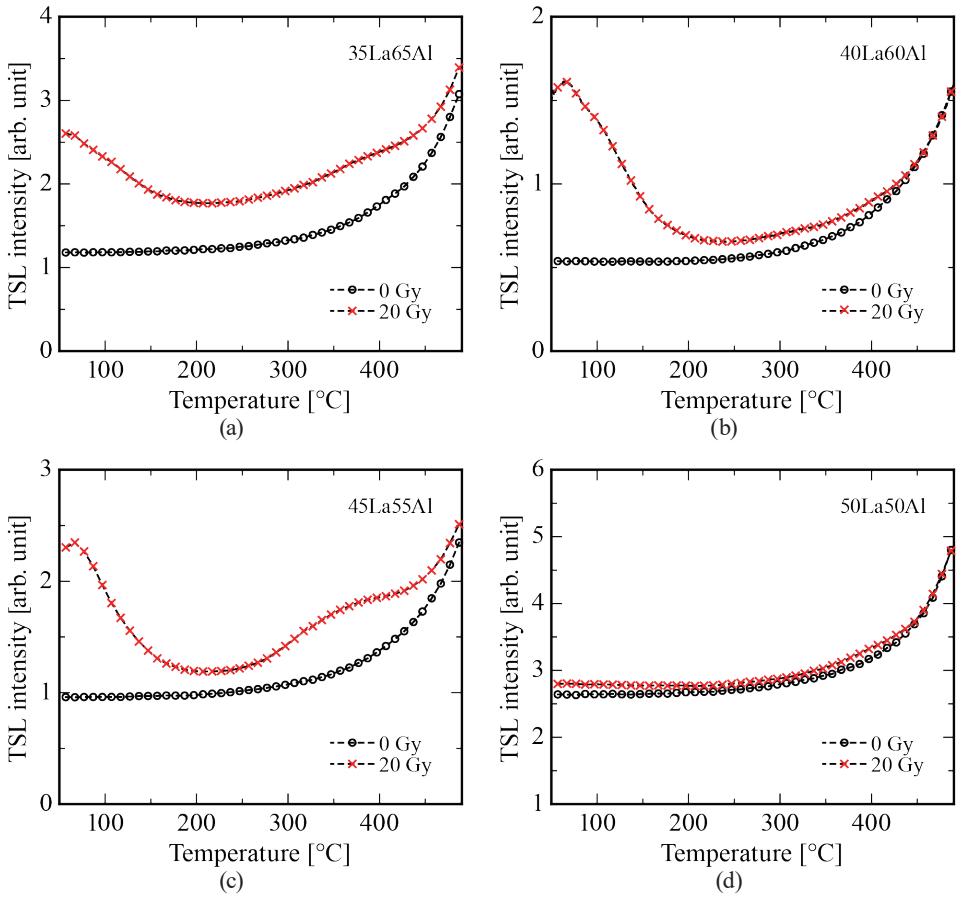

Fig. 8. (Color online) TSL glow curves of Ce-doped La_2O_3–Al_2O_3 glasses before/after 20 Gy of X-ray irradiation: (a) 35La65Al, (b) 40La60Al, (c) 45La55Al, and (d) 50La50Al.

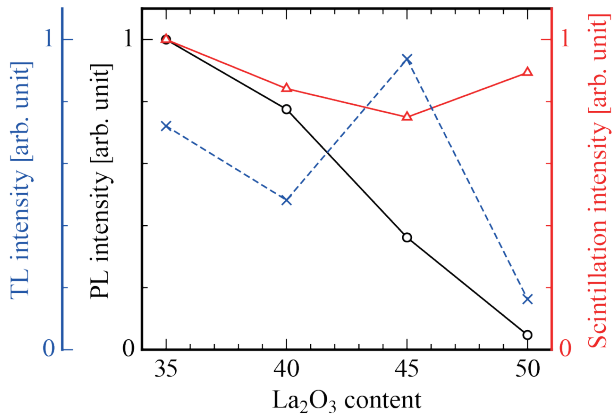

Fig. 9. (Color online) Correlation of PL intensity (open circles), scintillation intensity (open triangles), and TSL intensity (crosses) as a function of La_2O_3 content of Ce-doped La_2O_3–Al_2O_3 glasses.

when a glass composition has the same stoichiometry as an existing crystal, the arrangement of cations and oxygen ions tends to be highly similar.[59] In other words, the structure is relatively

close to a thermally equilibrated state, like that of a crystal, and is thus likely to have fewer structural defects. Consequently, we believe that the scintillation intensity increased, while the TSL intensity decreased, in the 50La50Al sample. The results suggest that this material can function as both a scintillator and a dosimeter material through structural control by precise composition design.

4. Conclusions

In this study, Ce-doped La_2O_3–Al_2O_3 glasses were prepared by the levitation method, a containerless glass-making method, and their optical and radiation-induced luminescence properties were investigated. The Raman spectra reveal that as La_2O_3 content increases, there is a notable increase in the number of NBO atoms owing to the reduction in the number of AlO_4 species, accompanied by a decline in the number of higher-coordination aluminum species, including AlO_5 and AlO_6. These results demonstrate alterations in the local structure of La_2O_3–Al_2O_3 glass induced by compositional changes. From the PL excitation and emission spectra, all samples exhibit broad visible emission under excitation at ~370 nm, with emission bands varying by glass composition. The 35La65Al and 40La60Al samples exhibited emission extending from 400 to 700 nm, while in the 45La55Al and 50La50Al samples, emission bands on the longer-wavelength side beyond 550 nm disappeared. On the basis of the results and PL lifetime measurements, the presence of at least two distinct emission species within this luminescence was revealed: one attributed to the 5*d*–4*f* transition of typical Ce^{3+} ions and the other associated with Ce–O associates. In the scintillation spectra, the luminescence from Ce–O associates was barely observed and the luminescence from the 5*d*–4*f* transition of Ce^{3+} was dominant. Furthermore, the scintillation spectra and TSL glow curve measurements indicated that the variations in glass composition had a significant effect on the transport efficiency of carriers generated by radiation. Therefore, the Ce-doped La_2O_3–Al_2O_3 glass can function as both a scintillator and a dosimeter material by optimizing the glass composition.

Acknowledgments

This work was supported by Grants-in-Aid for Scientific A (22H00309), Scientific B (22H02939), Early-Career Scientists (24K17504), and Research Activity Start-up (23K19188) from the Japan Society for the Promotion of Science.

References

1 S. Sharma, J. Baran, N. Chug, C. Curceanu, E. Czerwiński, M. Dadgar, K. Dulski, K. Eliyan, A. Gajos, N. Gupta-Sharma, B. C. Hiesmayr, K. Kacprzak, Ł. Kapłon, K. Klimaszewski, P. Konieczka, G. Korcyl, T. Kozik, W. Krzemień, D. Kumar, Sz. Niedźwiecki, D. Panek, S. Parzych, E. P. del Rio, L. Raczyński, S. Choudhary, R. Y. Shopa, M. Skurzok, E. Ł. Stępień, F. Tayefi, K. Tayefi, W. Wiślicki, and P. Moskal: EJNMMI Phys. **10** (2023) 28. https://doi.org/10.1186/s40658-023-00546-7

2 M. K. Singh: Radiography **30** (2024) 13. https://doi.org/10.1016/j.radi.2023.10.004

3 F. F. Alqahtani: Saudi Pharm. J. **31** (2023) 312. https://doi.org/10.1016/j.jsps.2022.12.013

4 A. Peacock, R. D. Andresen, E.-A. Leimann, A. E. Long, G. Manzo, and B. G. Taylor: Nucl. Instrum. Meth. **169** (1980) 613. https://doi.org/10.1016/0029-554X(80)90968-4

5 G. Della Casa, N. Zampa, D. Cirrincione, S. Monzani, M. Baruzzo, R. Campana, D. Cauz, M. Citossi, R. Crupi, G. Dilillo, G. Pauletta, F. Fiore, and A. Vacchi: Nucl. Instrum. Methods Phys. Res., Sect. A **1058** (2024) 168825. https://doi.org/10.1016/j.nima.2023.168825
6 S. Mianowski, N. De Angelis, K. Brylew, J. Hulsman, T. Kowalski, S. Kusyk, Z. Mianowska, J. Mietelski, D. Rybka, J. Swakon, and D. Wrobel: Exp. Astron. **56** (2023) 355. https://doi.org/10.1007/s10686-023-09906-8
7 Y.-Y. Ji, H.-Y. Choi, W. Lee, C.-J. Kim, H.-S. Chang, and K.-H. Chung: IEEE Trans. Nucl. Sci. **65** (2018) 2021. https://doi.org/10.1109/TNS.2018.2823322
8 M. Bakr, Z. G. Portakal-Uçar, M. Yüksel, Ü. H. Kaynar, M. Ayvacikli, S. Benourdja, A. Canimoglu, M. Topaksu, A. Hammoudeh, and N. Can: J. Lumin. **227** (2020) 117565. https://doi.org/10.1016/j.jlumin.2020.117565
9 J. S. Kim, P. Lee, B. R. Park, H. S. Kim, K. B. Kim, G. S. Cho, S. Shim, W.-H. Ha, S. Park, and Y.-W. Jin: Prog. Nucl. Sci. Technol. **6** (2019) 113. https://doi.org/10.15669/pnst.6.113
10 Y. Miyamoto, H. Nanto, T. Kurobori, Y. Fujimoto, T. Yanagida, J. Ueda, S. Tanabe, and T. Yamamoto: Radiat. Meas. **71** (2014) 529. https://doi.org/10.1016/j.radmeas.2014.08.007
11 J. Glodo, Y. Wang, R. Shawgo, C. Brecher, R. H. Hawrami, J. Tower, and K. S. Shah: Physics Procedia **90** (2017) 285. https://doi.org/10.1016/j.phpro.2017.09.012
12 L. E. Sinclair, D. S. Hanna, A. M. L. MacLeod, and P. R. B. Saull: IEEE Trans. Nucl. Sci. **56** (2009) 1262. https://doi.org/10.1109/TNS.2009.2019271
13 V. D. Ryzhikov, A. D. Opolonin, P. V Pashko, V. M. Svishch, V. G. Volkov, E. K. Lysetskaya, D. N. Kozin, and C. Smith: Nucl. Instrum. Methods Phys. Res., Sect. A **537** (2005) 424. https://doi.org/10.1016/j.nima.2004.08.056
14 A. Bala, D. G. Jenkins, and S. Namadi: DUJOPAS **8** (2022) 80. https://doi.org/10.4314/dujopas.v8i2a.9
15 T.-C. Wang, S.-Y. Yao, S.-P. Yan, J. Yu, Z.-Y. Deng, A. N. Yakovlev, B. Meng, J.-B. Qiu, and X.-H. Xu: ACS Appl. Mater. Interfaces **15** (2023) 23421. https://doi.org/10.1021/acsami.3c02041
16 I. Han and G. Kim: Nucl. Instrum. Methods Phys. Res., Sect. A **1064** (2024) 169397. https://doi.org/10.1016/j.nima.2024.169397
17 T. Yanagida, K. Kamada, Y. Fujimoto, H. Yagi, and T. Yanagitani: Opt. Mater. **35** (2013) 2480. https://doi.org/10.1016/j.optmat.2013.07.002
18 D. Shiratori, H. Fukushima, D. Nakauchi, T. Kato, N. Kawaguchi, and T. Yanagida: Sens. Mater. **35** (2023) 439. https://doi.org/10.18494/SAM4140
19 P. Kantuptim, T. Kato, D. Nakauchi, N. Kawaguchi, K. Watanabe, and T. Yanagida: Sens. Mater. **35** (2023) 451. https://doi.org/10.18494/SAM4141
20 Y. Oshima, T. Yasumune, T. Masuda, K. Maehata, K. Ishibashi, and T. Umeno: Prog. Nucl. Sci. Technol. **1** (2011) 296. https://doi.org/10.15669/pnst.1.296
21 D. Nakauchi, F. Nakamura, T. Kato, N. Kawaguchi, and T. Yanagida: Sens. Mater. **35** (2023) 467. https://doi.org/10.18494/SAM4138
22 A. J. J. Bos and J. B. Dielhof: Radiat. Prot. Dosim. **37** (1991) 231. https://doi.org/10.1093/oxfordjournals.rpd.a081056
23 D. Shiratori, H. Masai, T. Kato, G. Okada, D. Nakauchi, N. Kawaguchi, and T. Yanagida: Sci. Rep. **10** (2020) 21403. https://doi.org/10.1038/s41598-020-78510-z
24 M. Koshimizu, K. Oba, Y. Fujimoto, and K. Asai: Sens. Mater. **36** (2024) 565. https://doi.org/10.18494/SAM4761
25 R. Tsubouchi, H. Fukushima, T. Kato, D. Nakauchi, S. Saijo, T. Matsuura, N. Kawaguchi, T. Yoneda, and T. Yanagida: Sens. Mater. **36** (2024) 481. https://doi.org/10.18494/SAM4763
26 V. E. Kafadar and K. F. Majeed: Thermochim. Acta **590** (2014) 266. https://doi.org/10.1016/j.tca.2014.06.015
27 T. Kato, D. Nakauchi, N. Kawaguchi, and T. Yanagida: Sens. Mater. **34** (2022) 653. https://doi.org/10.18494/SAM3682
28 S. W. S. McKeever: Nucl. Instrum. Meth. Phys. Res., Sect. B **184** (2001) 29. https://doi.org/10.1016/S0168-583X(01)00588-2
29 H. Nanto and G. Okada: Jpn. J. Appl. Phys. **62** (2023) 10505. https://doi.org/10.35848/1347-4065/ac9106
30 G. Ito, H. Kimura, D. Shiratori, D. Nakauchi, T. Kato, N. Kawaguchi, and T. Yanagida: Sens. Mater. **34** (2022) 685. https://doi.org/10.18494/SAM3681
31 T. Kato, H. Kimura, K. Okazaki, D. Nakauchi, N. Kawaguchi, and T. Yanagida: Sens. Mater. **35** (2023) 483. https://doi.org/10.18494/SAM4137
32 D. Shiratori, Y. Isokawa, H. Samizo, G. Okada, N. Kawaguchi, and T. Yanagida: J. Mater. Sci.: Mater. Electron. **30** (2019) 2464. https://doi.org/10.1007/s10854-018-0520-0
33 M. Moszyński, T. Ludziejewski, D. Wolski, W. Klamra, and L. O. Norlin: Nucl. Instrum. Methods Phys. Res., Sect. A **345** (1994) 461. https://doi.org/10.1016/0168-9002(94)90500-2

34 T. Yanagida, Y. Fujimoto, Y. Yokota, K. Kamada, S. Yanagida, A. Yoshikawa, H. Yagi, and T. Yanagitani: Radiat. Meas. **46** (2011) 1503. https://doi.org/10.1016/j.radmeas.2011.03.039
35 M. Moszyński, D. Wolski, T. Ludziejewski, M. Kapusta, A. Lempicki, C. Brecher, D. Wiśniewski, and A. J. Wojtowicz: Nucl. Instrum. Methods Phys. Res., Sect. A **385** (1997) 123. https://doi.org/10.1016/S0168-9002(96)00875-3
36 K. Ahmed, K. Dahane, N. M. Khaidukov, N. Alves, and L. O. Faria: Optik **127** (2016) 6009. https://doi.org/10.1016/j.ijleo.2016.04.079
37 N. Alves, W. B. Ferraz, and L. O. Faria: Braz. J. Radiat. Sci. **7** (2019) ENAN 2017. https://doi.org/10.15392/bjrs.v7i2A.805
38 M. Rizwan, S. Gul, T. Iqbal, U. Mushtaq, M. H. Farooq, M. Farman, R. Bibi, and M. Ijaz: Mater. Res. Express **6** (2019) 112001. https://doi.org/10.1088/2053-1591/ab4629
39 S. Fujita, S. Yoshihara, A. Sakamoto, S. Yamamoto, and S. Tanabe: Proc. SPIE Fifth Int. Conf. Solid State Lighting **5941** (2005) 594111.
40 S. Tanabe, S. Fujita, S. Yoshihara, A. Sakamoto, and S. Yamamoto: Proc. SPIE Fifth Int. Conf. Solid State Lighting **5941** (2005) 594112.
41 D. Chen, W. Xiang, X. Liang, J. Zhong, H. Yu, M. Ding, H. Lu, and Z. Ji: J. Eur. Ceram. Soc. **35** (2015) 859. https://doi.org/10.1016/j.jeurceramsoc.2014.10.002
42 C. J. Benmore and J. K. R. Weber: Adv. Phys.: X **2** (2017) 717. https://doi.org/10.1080/23746149.2017.1357498
43 A. Masuno: J. Physical Soc. Jpn. **91** (2022) https://doi.org/10.7566/JPSJ.91.091003
44 D. Shiratori, D. Nakauchi, T. Kato, N. Kawaguchi, and T. Yanagida: J. Non-Cryst. Solids **607** (2023) 122227. https://doi.org/10.1016/j.jnoncrysol.2023.122227
45 Y. Watanabe, A. Masuno, H. Inoue, Y. Yanaba, and K. Kato: Phys. Chem. Chem. Phys. **22** (2020) 19592. https://doi.org/10.1039/D0CP02778B
46 L.-G. Hwa, J.-G. Shiau, and S.-P. Szu: J. Non-Cryst. Solids **249** (1999) 55. https://doi.org/10.1016/S0022-3093(99)00300-2
47 C. Bilel, R. Jbeli, I. Ben Jemaa, Y. Dabaki, M. Alzaid, F. Saadallah, M. Bouaicha, and M. Amlouk: J. Mater. Sci.: Mater. Electron. **32** (2021) 5415. https://doi.org/10.1007/s10854-021-05264-3
48 J. Cui and G. A. Hope: J. Spectrosc. **2015** (2015) 1. https://doi.org/10.1155/2015/940172
49 X. Zhang, W. Yang, J. Zhang, J. Li, L. Jiang, and X. Qi: J. Non-Cryst. Solids **525** (2019) 119599. https://doi.org/10.1016/j.jnoncrysol.2019.119599
50 H. Kimura, T. Fujiwara, M. Tanaka, T. Kato, D. Nakauchi, N. Kawaguchi, and T. Yanagida: Sens. Mater. **35** (2023) 513. https://doi.org/10.18494/SAM4146
51 K. Ichiba, Y. Takebuchi, H. Kimura, D. Shiratori, T. Kato, D. Nakauchi, N. Kawaguchi, and T. Yanagida: Sens. Mater. **34** (2022) 677. https://doi.org/10.18494/SAM3680
52 E. M. Abou Hussein, S. E. Shaban, Y. S. Rammah, M. H. Misbah, and M. A. Marzouk: Sci. Rep. **14** (2024) 13673. https://doi.org/10.1038/s41598-024-63207-4
53 D. Shiratori, D. Nakauchi, T. Kato, N. Kawaguchi, and T. Yanagida: Sens. Mater. **32** (2020) 1365. https://doi.org/10.18494/SAM.2020.2740
54 A. L. N. Stevels: J. Electrochem. Soc. **125** (1978) 588. https://doi.org/10.1149/1.2131506
55 J. Pejchal, V. Babin, M. Buryi, V. Laguta, F. Hájek, J. Páterek, L. Procházková-Prouzová, L. Havlák, V. Czerneková, V. Vaněček, V. Doležal, J. Havlíček, K. Rubešová, P. Zemenová, A. Falvey, R. Král, V. Pankratov, and K. Chernenko: Mater. Adv. **3** (2022) 3500. https://doi.org/10.1039/D1MA01083B
56 L.-J. Yin, G.-Z. Chen, C. Wang, X. Xu, L.-Y. Hao, and H. T. (Bert) Hintzen: ECS J. Solid State Sci. Technol. **3** (2014) R131. https://doi.org/10.1149/2.0191407jss
57 P. Peter, L. Marek, M. Jan, and G. Ondrej: Ceram. Silik. **53** (2009) 52.
58 H. Inoue, A. Masuno, A. Saito, Y. Watanabe, K. Tokuda, Y. Saito, and J. Iihara: J. Ceram. Soc. Jpn. **128** (2020) 279. https://doi.org/10.2109/jcersj2.20043
59 E. Muller, K. Heide, and E. D. Zanotto: J. Non-Cryst. Solids **155** (1993) 56. https://doi.org/10.1016/0022-3093(93)90471-9